Annals of Biomedical Engineering, Vol. 31, pp. 1263–1278, 2003
Printed in the USA. All rights reserved.

0090-6964/2003/31(10)/1263/16/$20.00

Partitioning of Cortical and Deep Cytoskeleton Responses from Transient Magnetic Bead Twisting

VALÉRIE M. LAURENT, REDOUANE FODIL, PATRICK CAÑADAS, SOPHIE FÉRÉOL, BRUNO LOUIS, EMMANUELLE PLANUS, and DANIEL ISABEY

Inserm UMR S 492, Physiopathologie et Thérapeutique Respiratoires, Institut Supérieur des Biosciences de Paris, Université Paris-12, 94010, Créteil, France

(Received 20 March 2003; accepted 22 July 2003)

Abstract—We attempted to estimate in living adherent epithelial alveolar cells, the degree of structural and mechanical heterogeneity by considering two individualized cytoskeleton components, i.e., a submembranous ''cortical'' cytoskeleton and a ''deep'' cytoskeleton (CSK). F-actin structure characterizing each CSK component was visualized from spatial reconstructions at low and high density, respectively, especially in a 10-μm-cubic neighborhood including the bead. Specific mechanical properties (Young elastic and viscous modulus E and η) were revealed after partitioning the magnetic twisting cytometry response using a double viscoelastic ''solid'' model with asymmetric plastic relaxation. Results show that the cortical CSK response is a faster ($\tau_1 \leqslant 0.7$ s), softer (E_1: 63–109 Pa), moderately viscous (η_1: 7–18 Pa s), slightly tensed, and easily damaged structure compared to the deep CSK structure which appears slower ($\tau_2 \sim \frac{1}{2}$ min), stiffer (E_2: 95–204 Pa), highly viscous (η_2: 760–1967 Pa s), more tensed, and fully elastic, while exhibiting a larger stress hardening behavior. Adding drug depolymerizing actin filaments decreased predominantly the deep CSK stiffness. By contrast, an agent altering cell–matrix interactions affected essentially the cortical CSK stiffness. We concluded that partitioning the CSK within cortical and deep structures is largely consistent with their respective functional activities. © *2003 Biomedical Engineering Society.*
[DOI: 10.1114/1.1616932]

Keywords—Rheological model, F-actin, Cellular mechanical properties, Viscoelastic model, Plasticity, Micromanipulation, Cell culture, Spatial reconstructions.

INTRODUCTION

Mechanical properties of the cytoplasm are important determiners of cell shape and cell motility and can, therefore, influence many cellular functions including growth, migration, and division. Cellular stability, cell shape, and its adaptation to extracellular environment have been recognized to be largely determined by the internal cytoskeletal structure.[15,23] The cytoskeleton (CSK) is constituted by a complex, heterogeneous molecular lattice of biopolymers. Three basic types of interconnected microfilaments (actin filaments or F-actin, microtubules, and intermediate filaments) were shown to be responsible for the ''solid'' and ''prestessed'' cytoskeletal behavior, which was satisfactorily represented by a tensegrity model.[25,50,53,55] The ''internal'' CSK, presently called the ''deep'' CSK component, is a structure of biopolymers which links and transmits forces through large regions of the cytoplasm, as from the nucleus to surface adhesion receptors.[23] Because the CSK realizes a direct mechanical coupling between distant points of the cellular network, it participates in intracellular signaling by transmitting mechanical and/or biochemical information into the cell. Among the three cytoskeletal biopolymers, which differ by their own ultrastructure, mechanical properties, and specific molecular interactions with extracellular ligands, actin filaments, and the proteins that cross link the filaments, appear to be major contributors to the mechanical properties of the cytoplasm.[34,52] Actin filaments can be variably interconnected to form multiple types of filament assemblies, each with a defined architectural organization. The most cited actin-filament assemblies are stress fibers, filipodia, and lamelipodia, but dorsal arcs, and concave or convex bundles of actin filaments, as well as geodesic arrays or some other less obvious networks, are often reported.[29,48,49] Noteworthy, the CSK not only acts globally but also acts at smaller scales, e.g., by providing a cortical tension (via the so-called cortical CSK), which plays a major role in cell motility,[1] endocytosis,[45] and local accommodation of the cell to stress.[20] This ''cortical'' actin cytoskeleton is constituted of the spectrin/ankyrin/actin network associated with the inner side of the cell membrane. In adherent cells, it is a scarcely explored actin cytoskeletal substructure, although it has often been evoked for its implication in many cellular functions.[6,20] In the present study we consider that both the cortical

Address correspondence to Daniel Isabey, Equipe Biomécanique Cellulaire et Respiratoire, Inserm UMR S 492 8, rue du Général Sarrail, 94010, Créteil, France. Electronic mail: daniel.isabey@creteil.inserm.fr

CSK acting at a local scale, and the deep CSK acting at a larger scale, would contribute to cellular function but their respective contributions to mechanical/chemical loading likely depend on cell type, undergoing function and cellular environment. Due to the wide variety of actin filament assemblies, we postulated that the cortical and deep CSK components might contain a wide variety of possible architectural organizations and molecular interconnections, depending on the polymerization process, actomyosin coupling, or protein binding. We presently considered that to understand cellular functions, it is crucial to determine the heterogeneous response of the cytoskeletal structure and important to quantify the mechanical properties of these cortical and the deep cytoskeletal key components.

We thus attempted to estimate, in living adherent epithelial alveolar cells, the structural and mechanical differences between the two cytoskeletal substructures by attempting to individualize them. The prerequisite for such a study was to use a force–displacement method with a specific access to the cytoskeletal structure, while not altering cellular integrity or cellular attachment to the rigid substrate. The magnetic twisting cytometry (MTC), initiated by Wang *et al.*,[53] was used because it allows specific probing of the CSK via selected transmembrane mechanotransmitters linked to the F-actin CSK. As done in previous studies,[33,41–43,54,56] we used ferromagnetic microbeads (4.5 μm in diameter) coated with a synthetic arginine–glycine–aspartic acid (RGD) peptide in order to ensure a specific linkage to the integrins. The CSK response was analyzed during both the loading and the unloading periods on the basis of a new two-component cytoskeletal model that permits heterogeneity of the CSK response and an asymmetric plastic behavior during relaxation. Changes in either internal or external cellular conditions were studied by agents specifically altering intracellular (e.g., cytochalasin D which depolymerizes F-actin) and environmental conditions (e.g., a metalloproteinase which induces extracellular matrix degradation). We also attempted to relate the specific mechanical responses of each CSK compartment to their specific structure using staining of F-actin by rhodamine phalloïdine at two F-actin densities. On the whole, the structural and mechanical results support the idea that using more than one individualized CSK component provides an improved model of the complex CSK behavior. The proposed model can then be seen as a first step to describe the role of CSK heterogeneity in the mechanical behavior of living cells.

MATERIALS AND METHODS

A549 Alveolar Epithelial Cell Culture

A549 human alveolar epithelial cells (American Type Culture Collection, Rockville, MD) were grown to confluence in DMEM containing 10% FBS, 2 mM L-glutamine, 50 IU/ml penicillin, 50 μg/ml streptomycin, and incubated in a 5% CO_2–95% air atmosphere. Routine subcultures (passages 89–92) were performed at 1/20 split ratios by incubation with 0.025 g/100 ml trypsin–0.02 g/100 ml EDTA in calcium- and magnesium-free PBS for 10 min at 37 °C. For magnetic twisting cytometry experiments, 96 well bacteriologic dishes were coated with either fibronectin or type I collagen at a concentration of 5 μg/cm^2 for 3 h at room temperature. Cells were plated at the density of 50 $\times 10^3$ per well in complete medium with serum, 24 h before experiments, and incubated in serum-free medium with 1% of BSA for 30 min before magnetic twisting cytometry experiments.

Principle of Magnetic Twisting Cytometry

Magnetic twisting cytometry applied to CSK mechanical response was initially proposed by Wang *et al.*[53] Specific mechanical stress is applied to the cytoskeleton of adherent cells via ferromagnetic beads linked to transmembrane mechanoreceptors. The laboratory-made magnetic twisting cytometry device used in this study has been previously described.[33,41,56] Carboxyl ferromagnetic beads (4.0–4.5 μm diam, Spherotec Inc., IL) were coated with RGD peptide according to the company's procedure (Telios Pharmaceuticals Inc., CA). Before use, coated beads were incubated in serum-free medium supplemented with 1% BSA for at least 30 min at 37 °C to block nonspecific bindings. Beads were then added to the cells (40 μg per well) for 20 min at 37 °C in a 5% CO_2–95% air incubator. Unbound beads were washed away with serum-free medium–1% BSA supplemented with 25 mM HEPES. Microbeads were then magnetized using a 0.15 T uniform magnetic pulse (150 μs). This magnetic field is horizontal, i.e., parallel to the monolayer of adherent cells. A magnetic torque, T_{mag}, was then created by Helmholtz coils, which generate a vertical uniform magnetic field $\mathbf{H}$ ($H \leqslant 6.3$ mT), whose intensity is two orders of magnitude lower than the magnetization field, which avoids remagnetization. T_{mag} is equal to the product of the magnetic moment of the bead $\mathbf{m}$ and the applied field $\mathbf{H}$, (i.e., $T_{\mathrm{mag}} = \mu_0 m H \sin(\pi/2 - \theta(t))$, μ_0 being the permeability of the free space). This magnetic torque T_{mag} induces a bead rotation which is measured by a magnetometer that continuously measures the average projection of the bead remanent magnetic field $B(t)$ in the plane of the cell monolayer ($= B_0$ at $t = 0$, i.e., before bead twisting), i.e., $\langle \cos \theta(t) \rangle = B(t)/B_0$. The variations of $B(t)$, are measured with a magnetometer equipped with low noise probes, i.e., 0.14 nT, for a range of bead remanent magnetic of the order of 1 nT. The apparent bead rotation angle $\theta(t)$ is obtained from

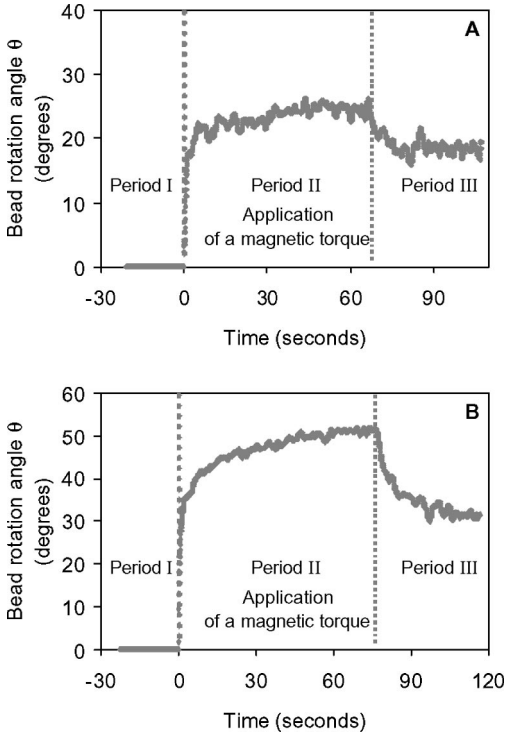

FIGURE 1. Typical curves of bead rotation angle θ (in degrees) vs. time (in seconds) without [in (A)] and with [in (B)] treatment with low concentrations of cytochalasin D in alveolar epithelial adherent cells. Beads coated with RGD are attached to integrin transmembrane mechanoreceptors. These response curves may be divided in three periods: (i) Period I (≈30 s) with no loading and no bead rotation ($\theta = 0°$). (ii) Period II (≈1 min) where a magnetic torque (of about 1000 pN×μm, in this case) was applied, generated by a constant perpendicular magnetic field. In response to this torque, beads initially rotate, to reach a plateau which suggest a viscoelastic "solid" behavior. (iii) Period III (≈30 s), the magnetic torque is switched off and CSK response is characterized by a partial recovery of the initial bead position, which indicates a plastic behavior.

$$\theta(t) = \cos^{-1}[B(t)/B_0]. \quad (1)$$

Note that the apparent angle measured by MTC, i.e., $\cos^{-1}(\langle\cos\theta(t)\rangle)$, may differ from the actual mean rotation angle $\langle\theta(t)\rangle$,[13] likely due to the nonlinearity of the function $\cos^{-1}$. The partial bead immersion in the cellular medium was estimated from three-dimensional reconstructions of the actin cytoskeleton following a method previously described by Laurent *et al.*[33] Figure 1 shows two typical curves of the bead rotation angle θ as a function of time t for cells treated or not treated with cytochalasin D. These curves comprise three phases: (i) the resting period before loading (period I) corresponding to $\theta(t) = 0$; (ii) the loading period (period II) in which the bead rotation angle rapidly increases to reach a plateau within a minute of load application; and (iii) the unloading period (period III) is a relaxation period immediately following interruption of the magnetic torque, the latter period being characterized by only partial recovery of the initial bead position.

Analysis of the CSK Response with Standard and Proposed Rheological Models

The bead rotation angle at reference state [Fig. 1(A)] and during actin depolymerization [Fig. 1(B)] were analyzed both in the loading phase and immediately after cessation of loading, i.e., the relaxation period (period III). To take into account the incomplete recovery of bead position, which characterizes period III in Fig. 1, we tested by least-squared adjustments rheological models, which purposely include a serial arrangement of viscous and/or plastic elements, which are known to commonly lead to a lack of full recovery. Tested elementary models represented: (i) viscoelastic "fluid," i.e., a Voigt body in series with a dashpot [Figs. 2(A) and 2(B)], or a Kelvin (or Zener) body in series with a dashpot [Figs. 2(C) and 2(D)], (ii) a viscoelastic "solid," i.e., the unique Voigt body classically used to analyze MTC data [Figs. 2(E) and 2(F)], and a two-component viscoelastic "solid" model with asymmetric plastic relaxation [Figs. 2(G) and 2(H)], which includes a first Voigt body, with a parallel plastic element exclusively added in the post-loading period, in series with a second Voigt body. Note that fluid models, i.e., in Figs. 2(A)–2(D), well fitted period II but failed to fit period III, while the nonplastic viscoelastic solid model [Figs. 2(E) and 2(F)] failed to fit both periods II and III. Thus, nonplastic models were not retained below for further analysis of the CSK response in MTC. Similarly, a large class of other simple solid or fluid models were eliminated since they could not fit either period II or III or both, e.g., the well-known Maxwell model which shows an infinitely sharp jump in bead rotation and infinitely sharp decay in relaxation followed by a constant rotation angle much below the experimental plateau value (data not shown), or the Kelvin body in series with a dashpot [Figs. 2(C) and 2(D)], which has been previously proposed to describe pulse magnetic bead microrheometry,[4] but failed to describe the relaxation period in our experiments (period III in Fig. 1). This is why we retained the two-component viscoelastic model with asymmetric plastic relaxation, which is described below.

Proposed Two-Component Viscoelastic Model with Asymmetric Plastic Relaxation

The proposed two-component viscoelastic model with asymmetric plastic relaxation [shown in Figs. 2(G) and 2(H)] is such that the two Voigt bodies are submitted to the same magnetic torque. Due to partial immersion of the bead in the cytoplasm during MTC, the magnetic torque T_{mag} corresponds to a constant corrected stress

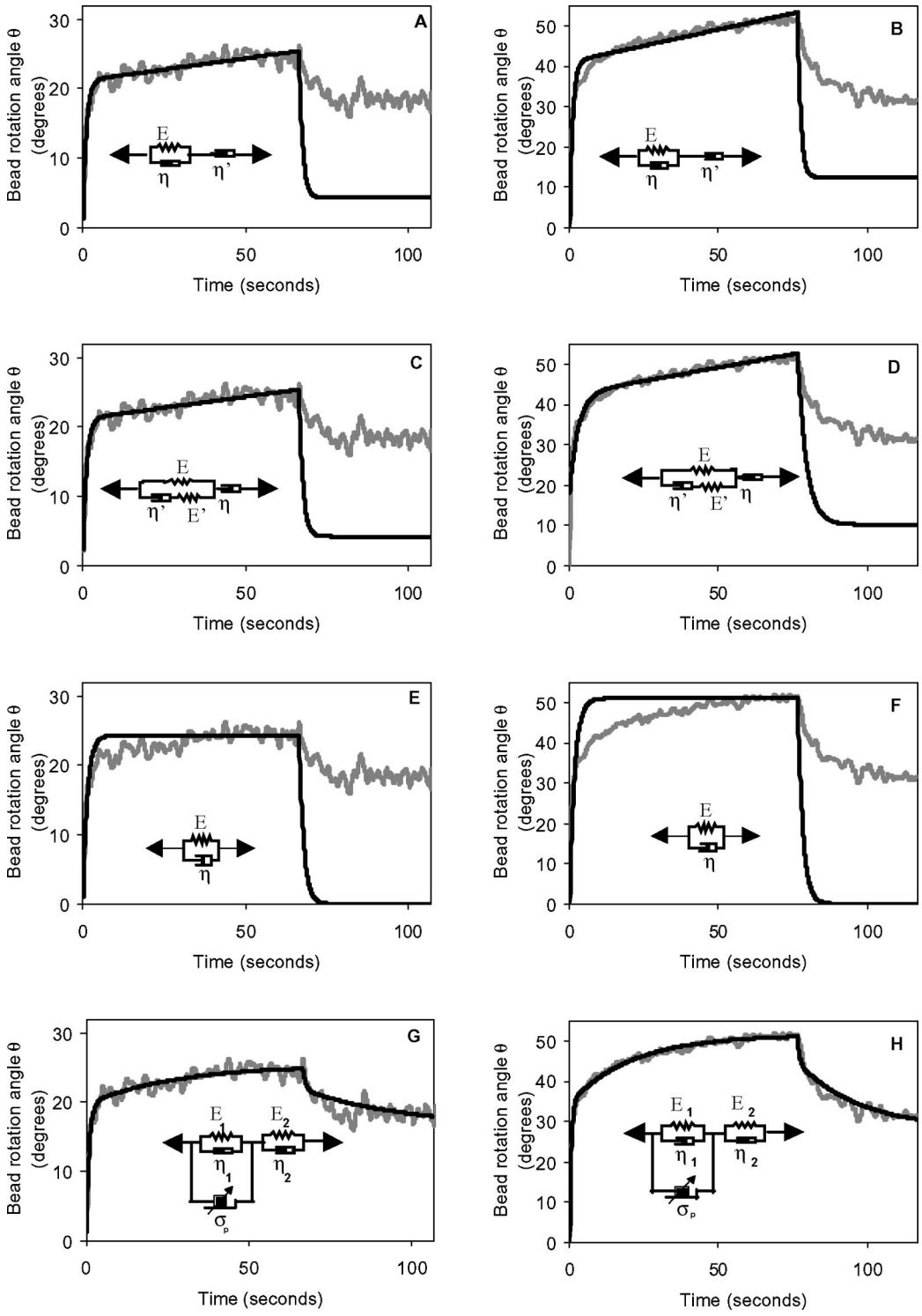

FIGURE 2. Curve fitting analysis of experimental curves (gray curves of periods II and III shown in Fig. 1 above) with various rheological models (black curves) without cytochalasin D [i.e., graphs (A), (C), (E), and (G) in the left column] and during a cytochalasin D treatment, which produces actin depolymerization [i.e., graphs (B), (D), (F), and (H), in the right column]. In the four upper graphs (A)–(D), classical viscoelastic "fluid" models are tested: in (A) and (B), a Voigt body in series with a dashpot, and (C) and (D), a Kelvin (or Zener) body in series with a dashpot. In (E)–(F), a viscoelastic "solid" model made of a unique Voigt body is tested, as classically done with the MTC technique. In (G) and (H), the proposed model: "two-component viscoelastic model with asymmetric plastic relaxation" includes, during loading, a series of two Voigt bodies and during unloading, the same model modified by a plastic element added in parallel to Voigt body No. 1 (the rapid component) in order to take into account bead-induced cellular damage and/or remodeling.

given by $\sigma_0[=T_{mag}/(V\sin^3\alpha)]$. V is the bead volume. α is the half angle of bead immersion and was taken to be 67° as estimated in Ref. 33. The two components complementarily contribute to bead rotation, leading to the specific estimation of viscoelastic properties for the two CSK components. Then, in the loading period, the equations of instant equilibrium for the two CSK components are:

$$\theta(t)=\theta_1(t)+\theta_2(t), \tag{2a}$$

$$\sigma_0=E_1\theta_1(t)+\eta_1\dot{\theta}_1(t), \tag{2b}$$

$$\sigma_0=E_2\theta_2(t)+\eta_2\dot{\theta}_2(t), \tag{2c}$$

where θ_1 and θ_2 are the displacements of the two CSK components, with $\theta(t)=\theta_1(t)=\theta_2(t)=0°$ at $t=0$. E_1 and E_2 are the elastic modulus and η_1 and η_2 are the viscosity modulus of, respectively, the rapid and the slow CSK components.

In the unloading period, the only partial recovery of bead position is taken into account in the model by adding, as soon as relaxation starts, i.e., at the maximal value of total elastic recoil stress [defined by $\sigma_{max}=E_1\,\theta_1(t_{off})+E_2\,\theta_2(t_{off})$, at the exact instant of loading release $t=t_{off}$], a parallel plastic element [shown in Figs. 2(G) and 2(H), which hinders relaxation of the rapid CSK components below a certain level of elastic recoil stress σ called plastic threshold stress σ_p, i.e., $\sigma\leqslant|\sigma_p|$, corresponding to the time interval ($t\geqslant t_p$), where t_p is the plastic threshold time. Addition of this plastic element in parallel to the rapid Voigt body allows the two viscoelastic components to contribute to the relaxation of the system but only in the early phase of relaxation (i.e., $\sigma\geqslant|\sigma_p|$ corresponding to $t_{off}\leqslant t\leqslant t_p$). Beyond $\sigma=|\sigma_p|$, permanent deformation occurs for the rapid component, i.e., the elastic recoil of this component is impeded and the relaxation is uniquely provided by the slow component of the model. Thus, during unloading ($t\geqslant t_{off}$), Eq. 2(a) is still valid but Eqs. 2(b) and 2(c) are modified as follows:

$$\theta_1(t)=\theta_p \quad \text{for} \quad \sigma\leqslant|\sigma_p|\text{corresponding to } t\geqslant t_p, \tag{3a}$$

$$E_1\theta_1(t)+\eta_1\dot{\theta}_1(t)+\sigma_p=0, \tag{3b}$$

$$E_2\theta_2(t)+\eta_2\dot{\theta}_2(t)=0. \tag{3c}$$

The plastic threshold stress can be calculated by

$$|\sigma_p|=E_1\theta_p. \tag{4}$$

It corresponds to the time where the viscous term gets zero because the time derivative of the rotation angle gets zero, leading to $\theta_1(t_p)=\theta_p=$ constant, i.e., the plastic threshold stress equilibrates the elastic recoil stress.

The equation system [Eqs. (2) and (3)] describing the behavior of the two-component model with asymmetric plastic relaxation has been solved analytically. During the loading period, assuming constant the magnetic torque, rotation angle θ is given by

$$\theta(t)=a_1(1-e^{-t/\tau_1})+a_2(1-e^{-t/\tau_2}). \tag{5}$$

During the unloading period, the solution of the equation system (2a) and (3a)–(3c) is

$$\begin{aligned}\theta_r(t)=&-a_p(1-e^{-(t-t_{off})/\tau_1})\\&+a_1(1-e^{-t_{off}/\tau_1})e^{-(t-t_{off})/\tau_1}\\&+a_2(1-e^{-t_{off}/\tau_2})e^{-(t-t_{off})/\tau_2}.\end{aligned} \tag{6}$$

The two first terms of Eq. (6) represent the contribution of the viscoplastoelastic relaxation of component No. 1 while the third term represents the contribution of the viscoelastic relaxation of component No. 2. Parameters in Eq. (6) are related to elastic and plastic properties as follows:

$$a_p=\frac{\sigma_p}{E_1}, \quad a_1=\frac{\sigma_{max}}{E_1}, \text{ and } a_2=\frac{\sigma_{max}}{E_2}. \tag{7}$$

a_p, a_1, a_2, τ_1, and τ_2 were determined by curve fitting analysis of experimental curves $\theta(t)$ by Eq. (2) using Kaleidagraph software. In Eqs. (2a)–(2c) above, the time constants τ_1, τ_2 are equal to the ratio of viscosity modulus to elasticity modulus. However, we recently proposed to correct these relationships in order to take into account the actual MTC probing conditions, e.g., degree of bead immersion.[33] Accordingly, we have used

$$\eta_1=\frac{E_1\cdot\tau_1}{3} \quad \text{and} \quad \eta_2=\frac{E_2\cdot\tau_2}{3}. \tag{8}$$

Young elasticity moduli E_1 and E_2, and viscosity moduli η_1 and η_2 were deduced from Eqs. (7) and (8) and are plotted in Table 1 for four different values of applied stress (i.e., 13, 23, 31, and 38 Pa). Plastic threshold stress σ_p was calculated from Eq. (4) after estimating θ_p from slope changes in the unloading period, e.g., see period III in Fig. 1 or in Fig. 2(G), and plotted in Table 1.

TABLE 1. Mean values ± s.e.m. of mechanical properties[a] of studied cells. All data are based on eight experimental points excepted when the number of experimental points is indicated in parentheses.

A				
Initial stress σ_0	13 Pa	23 Pa	31 Pa	38 Pa
E_1 (Pa)	63±5	77±5	83±5	109±8
E_2 (Pa)	95±10	160±12	204±8	202±13
η_1 (Pa s)	7±1	16±1	18±2	14±1
η_2 (Pa s)	760±131	1345±194	1967±127	971±105
τ_1 (s)	0.3±0.1	0.7±0.1	0.7±0.1	0.4±0.1
τ_2(s)	23±2	25±4	30±3	14±1
σ_p (Pa)	13±1	22±1	27±1	37±1 (n=3)
B				
Initial stress σ_0	13 Pa	23 Pa	31 Pa	38 Pa
E_1 (Pa)	32±2	47±2	58±2	73±3
E_2 (Pa)	49±3	87±3	104±2	121±6
η_1 (Pa s)	7±1	12±1	11±1	18±1
η_2 (Pa s)	482±62	786±49	824±62	885±169
τ_1 (s)	0.4±0.1	0.8±0.1	0.6±0.1	0.6±0.1
τ_2(s)	29±3	28±2	24±2	21±3
σ_p (Pa)	10±1	16±1 (n=7)	23±1	28±3 (n=3)

[a]Elasticity modulus E (in Pa), viscosity modulus η (in Pa s), time constant τ (in s), and plastic threshold stress σ_p (in Pa) at various levels of initial stress σ_0 (=13, 23, 31, and 38 Pa) for cytoskeleton components "1" (rapid/cortical) and "2" (slow/deep) obtained in cultured adherent epithelial alveolar cells, twisted with magnetic beads, at basal state [Table 1(A)] and during treatment with a depolymerizing agent (cytochalasin D) [Table 1(B)].

Effect of Actin Depolymerization

To evaluate the effect of changing intracellular conditions on the mechanical behavior of the two CSK networks, we used low concentrations (1 μg/ml) of cytochalasin D, which specifically depolymerizes the F-actin cytoskeleton. For such a concentration used on epithelial adherent cells, this drug has been previously reported to decrease CSK internal tension without markedly changing cell attachment and cell shape.[56] To study the effect of actin depolymerization on the mechanical properties of each CSK component of epithelial adherent cells, we analyzed the CSK response with the two-component model in untreated cells and in cells treated with a low concentration of cytochalasin D. As in that previous study, adherent cells were plated onto fibronectin in culture wells and cytochalasin D treatment lapsed 20 min before the measure of cell mechanical properties by magnetic twisting cytometry.

Effect of Enzymatic Degradation of Extracellular Matrix

Changes in extracellular conditions were obtained by adding exogeneous recombinant pro-MMP-13 (collagenases) over epithelial cells plated on collagen. Pro-MMP-13 were expressed by stable transfection of NSO mouse myeloma cells and purified from serum-free conditioned cell culture medium, as previously described.[31,40] The effect of collagenases on CSK mechanical properties previously tested using the standard single Voigt model[41] was reexamined on the basis of the proposed two CSK component model. This effect, which is known to degrade the extracellular matrix, was tested by plating cells in DMEM containing collagenase 24 h before applying magnetic twisting cytometry. Two concentrations of pro-MMP, 50 and 250 ng/ml were used.

Statistical Analysis

For experiments performed with the same wells, differences between two groups of values were tested with paired two-sided Student's t-test whereas, for experiments performed on different wells, differences between two samples were tested with two-sided Student's t-test. $p<0.05$ was considered significant. Results are presented as means ± s.e.m.

Three-Dimensional Reconstructions of Cortical and Deep Actin CSK

The CSK structure of the studied adherent epithelial cells was evidenced by staining F-actin with fluorescent phallotoxin following a method described in a previous study.[56] The stained F-actin CSK structure was examined with a ×100/1.3 numerical aperture Plan Neofluar objective mounted on a laser confocal microscopy (LSM 410, Zeiss, Rueil-Malmaison, France). Accurate representation of the spatial organization of F-actin structure was obtained from three-dimensional (3D) reconstructions performed from optical sections recorded every 0.25 μm, which revealed intracellular fluorescence by means of a gray level scale.

Preliminary to the 3D reconstruction, a deconvolution process was performed on the stack of gray level images (8 bits) by the appropriate software's module AxioVision 3.0.6 (Carl Zeiss, NY) that allows correcting the distortion due to the optical system of the confocal microscope. The deconvolution process uses a mathematical algorithm, which takes into account the theoretical point spread function (PSF) calculated for each acquisition parameter. The fixed images data are implemented at the right scale in Amira 2.3 software (TGS Inc., CA), which uses the threshold segmentation method to extract cell contours. Contours of external and internal subcellular structures corresponding to different levels of fluorescent intensity were defined using the curve of the ''logarithmic'' decrease in cumulated pixels of the stack images versus the gray level (0–255). Practically, the cell image ranged from 8 to 169. The lower value detectable (i.e., 8) corresponded to the external boundary of the actin struc-

ture while the deep CSK structure was systematically defined at an arbitrary value located at 25% of that range (i.e., ~40). The 3D reconstruction of each structure was performed by a generalized marching cube (GMC) module (GMC algorithm) of Amira software, which generates, using a triangulation method, an isosurface from segmented optical plans. Visualization of the 3D reconstructed cells was performed using 3D-Studio Max v3.1 software (Kinetix, CA), allowing calculation of the volume from a surface.

To characterize the representative F-actin neighborhood of beads, we considered the 3D reconstructions of the dense and less dense CSK structures in a close neighborhood of a few beads. The relative amount of dense F-actin was estimated in a parallelpiped embedding the bead with a base of about $12\times 9\ \mu$m and a height depending on cell thickness. Although the bead surface was not specifically marked in these experiments, we spatially reconstruct the bead position in the cell using spheres whose size and location were precisely determined, either during direct confocal microscopy or during postacquisition from cell images stored in interferential contrast Nomarski. The volume occupied by the dense F-actin structure was then calculated and compared to the overall volume of F-actin structure, which corresponds to the lowest F-actin density.

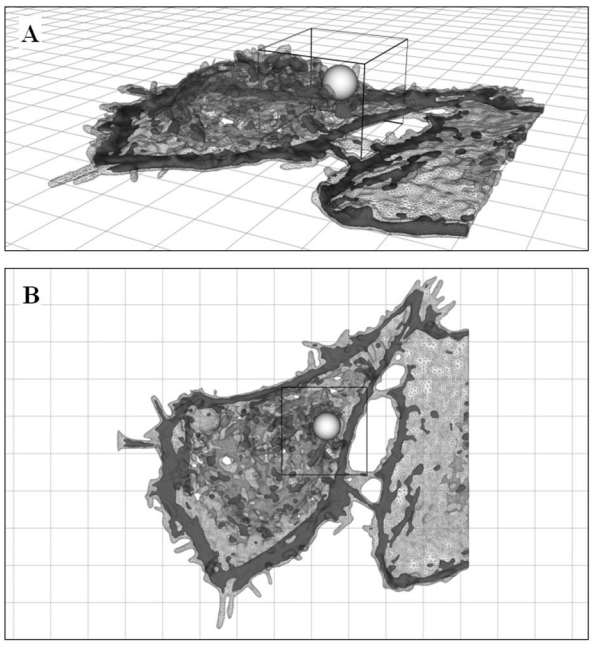

FIGURE 3. Oblique (A) and apical (B) views of three-dimensional reconstructions of fixed adherent epithelial cells probed by a microbead and stained for F-actin with rhodamine phalloïdine. The two fluorescent intensity levels used reveal a "deep" actin CSK structure with a high fluorescent F-actin intensity (dark gray), and a submembranous "cortical" actin CSK structure with a low fluorescent F-actin intensity (light transparent gray).

RESULTS

Spatial Reconstruction of CSK Structures at Low and High F-Actin Density

The three-dimensional F-actin CSK structures, reconstructed at two density levels in a given adherent epithelial alveolar cell, are presented in Figs. 3(A) (oblique view) and 3(B) (apical view). The dense F-actin structure [dark gray in Fig. 3(B)] provides an overall view of the deep CSK organization of F-actin, mainly constituted by the dense F-actin assemblies such as stress fibers whose peripheral organization, by linking far regions of the cytoplasm between focal adhesions, is clearly visible in this cell. By contrast, the F-actin structure with the lowest density [the transparent grid in light gray in Fig. 3(B)] appears to surround the entire cell as a thin mantle, from 0.5 to 2 μm thick (later shown in Fig. 4). Note that this low density F-actin structure is externally bounded by the cytoplasmic face of the membrane and internally by the nonactinic intracytoplasmic elements, including the nucleus. In the 3D reconstructions of Fig. 3(B), the deep and surrounding CSK structures appear intimately connected since the dense F-actin structure is embedded in a surrounding F-actin structure, the transcellular or intracellular differences coming from the variability of the relative volume of dense F-actin structure compared to the less dense F-actin structure. We presently postulate that the volumetric fraction of dense (and less dense) F-actin structure relatively to the overall F-actin structure conditions the overall mechanical response of the cell.

To analyze in more detail the F-actin structure around a representative sample of beads [see the cubic volume shown in Figs. 3(A) and 3(B)], we examined the 3D reconstructions of F-actin structures pertaining to the deep and cortical CSK structures in the vicinity of 22 beads pertaining to different cells and covering a variety of local actin-cytoskeleton assemblies (e.g., apical, basal, peripheral, central, etc.). Such a variety is illustrated by the four local actin structures shown in Figs. 4(a)–4(h). We also calculated the volumetric fraction (noted δ) of dense F-actin structure relatively to the total volume F-actin structure present in the cubic neighborhood of the 22 beads tested (Fig. 5). For the 22 cases tested, individual values of δ were in the range 7%–42%, and a roughly Gaussian distribution with an average value at 18%. Note that the percentage of dense F-actin (δ) was never zero, showing that dense and less dense actin structures were always present (but in variable proportion) in the vicinity of the 22 beads tested [Figs. 4(a)–4(h)]. This suggests that each bead may sense both dense and less dense CSK components, but in a variable proportion depending on bead location in the cell and beyond on cell type and function. In Fig. 4, the volumetric fraction, δ, decreases from the top to the bottom, i.e.,

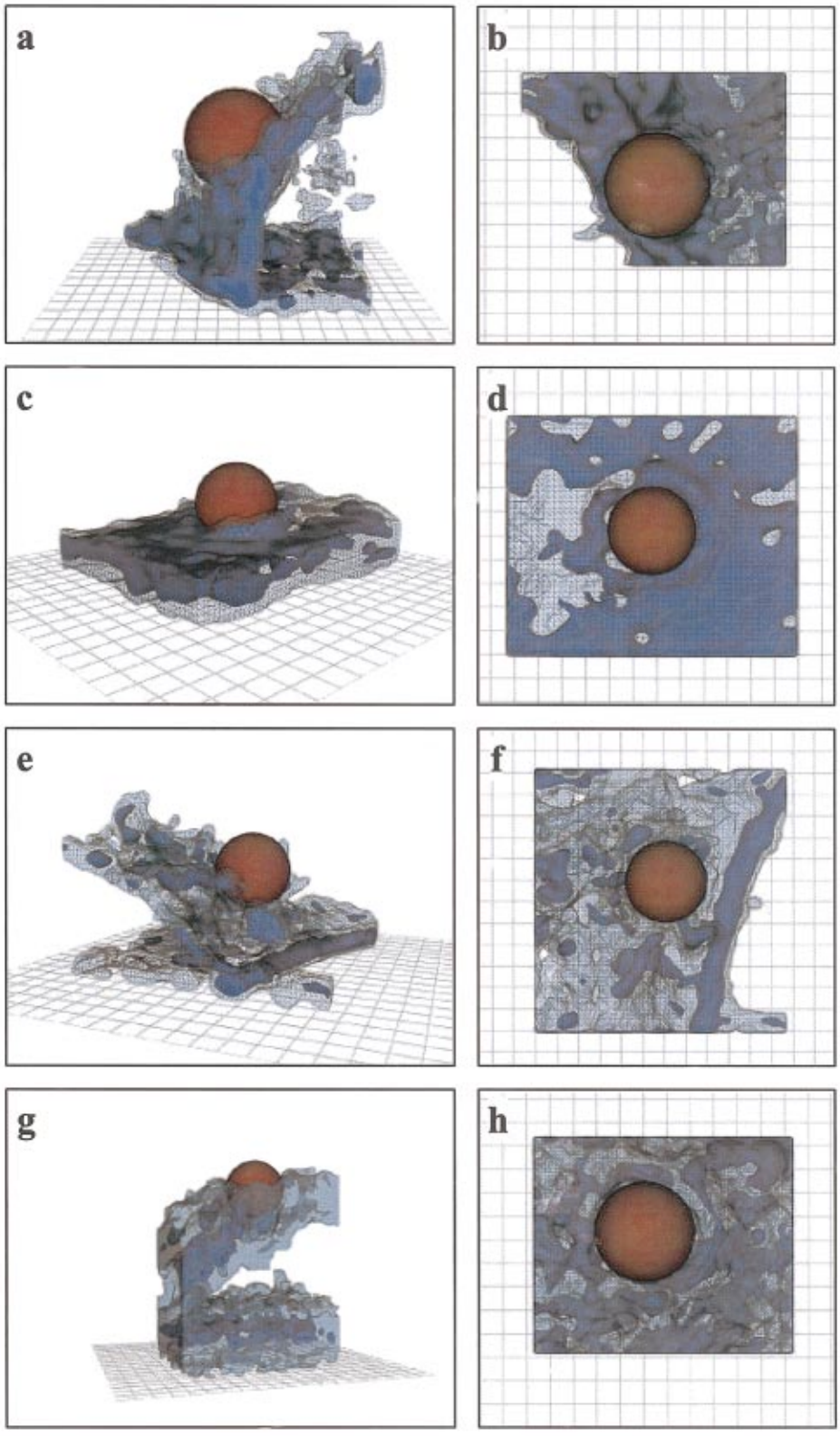

FIGURE 4. Oblique [(a), (c), (e), and (g)] and apical [(b), (d), (f), and (h)] views of three-dimensional reconstructions of fixed adherent epithelial cells probed by microbeads and stained for F-actin with rhodamine phalloïdine in cubic neighborhoods including the bead. The two fluorescent intensity levels used reveal a "deep" actin CSK structure with a high fluorescent F-actin intensity (dark blue), and a submembranous "cortical" actin CSK structure with a low fluorescent F-actin intensity (light blue grid). From top [(a) and (b)] to bottom [(g) and (h)] there is a decreasing amount of the fraction of the volume occupied by the dense F-actin structure relatively to the total volume of F-actin structure in each considered bead neighborhood. Structures in (a) and (b) correspond to the case where the fraction of local volume occupied by the dense F-actin is maximal (i.e., 42%). This corresponds to a case where bead position in the cell is at the same time more peripheral and near the basal face, hence, the predominance of dense F-actin in the bead neighborhood. In (c) and (d), the fraction of local volume occupied by the dense actin is smaller (i.e., 28%), because the highly spread shape of the cell makes the bead closer from the basal face. In (e) and (f) the fraction of local volume occupied by the dense actin is largely reduced (i.e., 11%), even minimal in (g) and (h) (i.e., 7%). The side of each square on the horizontal reference plane represents 1 μm.

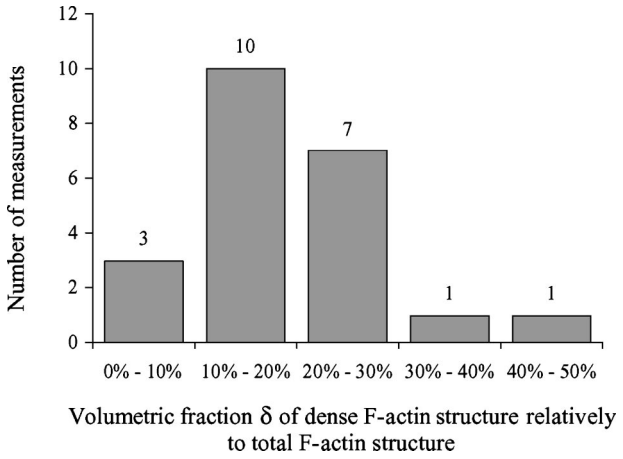

FIGURE 5. Number of measurements corresponding to different values of the volumetric fraction (δ) of dense F-actin structure relative to total F-actin structure in the bead neighborhood (see the text for explanation).

from 42% in Figs. 4(a) and 4(b) down to 7% in Figs. 4(g) and 4(h). Although the low density F-actin structure is largely predominant for the two lower cases [Figs. 4(e) and 4(h)], the bead appears still connected to a few isolated stress fibers of dense polymerized actin. Altogether, F-actin 3D reconstructions suggest that a mechanical continuum always exists between the bead and the more and the less dense F-actin network, but the volumetric fraction between each CSK component greatly varies.

Mechanical Properties of the Cortical and Deep CSK Components

Mechanical properties of the cytoskeleton of adherent epithelial alveolar cells, untreated and treated with the actin depolymerizing drug (cytochalasin D) as well as by enzymatic degradation of extracellular matrix, were obtained by least-square adjustment on experimental curves of the two-component viscoelastic model with asymmetric plastic relaxation [shown in Figs. 2(G) and 2(H) for a given level of stress, i.e., $\sigma_0 = 23$ Pa]. Mechanical properties are summarized in Tables 1(A) and 1(B). The mechanical property dependence on stress level is shown in Figs. 6(A)–6(D) for viscoelastic properties and Fig. 8 for plastic properties. Elastic modulus (E_1 and E_2) and viscosity modulus (η_1 and η_2) were obtained in the loading period (II in Fig. 1), and values were maintained in the

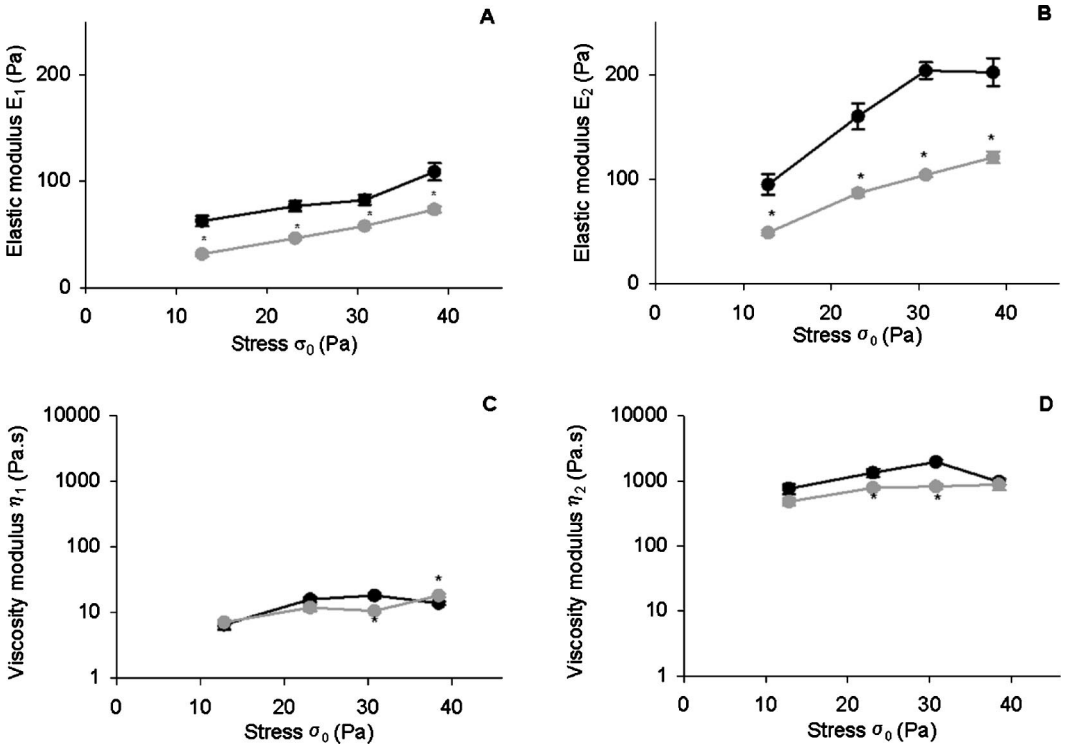

FIGURE 6. Graphs showing the effect of depolymerization of actin filaments by adding cytochalasin D. Without cytochalasin D (dark symbols), with cytochalasin D (gray symbols). (A) Elastic modulus of the rapid cortical CSK component, E_1 in Pa. (B) Elastic modulus of the slow deep CSK component, E_2 in Pa. (C) Viscosity modulus of the rapid component (cortical CSK component), η_1 plotted on a logarithmic scale in Pa s. (D) Viscosity modulus of slow deep CSK component, η_2 plotted on a logarithmic scale in Pa s. Values are mean ±s.e.m. and $n = 8$ wells for each points [except in three cases (indicated in Table 1)]; *$p < 0.05$, means a significant difference between untreated and treated cells.

postloading period with the difference that a plastic threshold stress σ_p was added to the rapid component in the relaxation period. Table 1(A), Fig. 6, and Fig. 8 show that, depending on values of stress σ_0 applied, the two CSK components systematically exhibit different behaviors in terms of time response and mechanical properties. Indeed, time constants differed by more than one order of magnitude ($\tau_1 \sim \frac{1}{2}$ s and $\tau_2 \sim \frac{1}{2}$ min) and are relatively insensitive to stress. The elastic modulus of the rapid CSK component was significantly smaller than the slow CSK component ($E_1 = 63-109$ Pa vs $E_2 = 95-204$ Pa), while the viscosity modulus of the rapid CSK component was more than two orders of magnitude smaller than the slow one ($\eta_1 = 7-18$ Pa s vs $\eta_2 = 760-1967$ Pa s). Note that the stress-hardening response, which means a stiffness–stress relationship with positive slope, was more marked for the slow than for the rapid CSK components [Figs. 6(A) and 6(B)]. Note, also, that the viscosity modulus of both CSK components [plotted on a vertical logarithmic scale in Figs. 6(C) and 6(D)] exhibits a tendency to increase with stress in the range of stress $\sigma_0 = 13-31$ Pa. Note that at the highest stress value tested ($\sigma_0 = 38$ Pa), elastic and viscosity moduli might be underestimated due to shift in the measured remanent magnetic signal (due to the raise of temperature in circuits) and/or limitations of the linear analysis (CSK response might become non linear) (see Ref. 33).

Effect on Each CSK Component of Depolymerizing F-Actin

Analysis by the two-component model of the CSK response after treatment by cytochalasin D did not deeply modify the time constant values of the two CSK components [see Table 1(B)], meaning that the discrepancies in time response observed at the basal state between the two CSK components were maintained during actin depolymerization. The elasticity modulus of the rapid and the slow CSK components appeared significantly and systematically reduced during cytochalasin D treatment [Figs. 6(A) and 6(B), respectively]. The stress-hardening response of the slow CSK component appeared considerably reduced in Fig. 6(B) while the cortical stress-hardening response did not seem to be affected in Fig. 6(A). For the lowest stress value tested (i.e., $\sigma_0 = 13$ Pa), the relative decrease in elasticity modulus induced by cytochalasin D was the same for the two CSK components, i.e., 49%. Above $\sigma_0 = 13$ Pa, the decrease in elasticity modulus for the rapid component was sensibly smaller than for the slow component, i.e., 39% vs 46% at 23 Pa, 30% vs 49% at 31 Pa, and 33% vs 40% at 38 Pa for the elasticity modulus decrease of the rapid versus the slow CSK component. The differences in terms of elasticity modulus measured before and during the cytochalasin D treatment have been used to estimate the CSK prestress at several levels of applied stress as previously performed.[41,43] Using the data in Figs. 6(A) and 6(B), it is easy to deduce that, for the four stress levels considered, CSK prestress was found to be smaller for the rapid CSK component than for the slow CSK component. Incidentally, cytochalasin D treatment had a larger effect on the viscosity modulus of the slow CSK component compared to the rapid CSK component, except at the higher stress value tested (38 Pa) (see above).

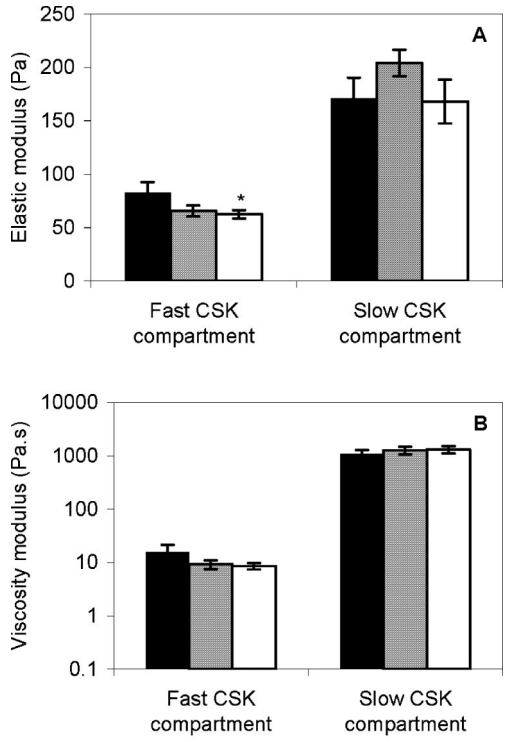

FIGURE 7. Effect of adding exogenous matrix metalloproteinase (MMP) on the mechanical properties of the two-actin networks. (a) Elasticity modulus (in Pa) measured for the two CSK components. (b) Viscosity modulus (in Pa s) of the two CSK components, without MMP (black bars), with 50 ng/ml of MMP (gray bars), and with 250 ng/ml of MMP (white bars). Values are mean ± s.e.m. and $n = 8$ wells for each point.

Effect on Each CSK Component of Enzymatic Degradation of Extracellular Matrix

Changing extracellular conditions was performed by adding an exogenous matrix metalloproteinases (collagenases) to epithelial cells culture and its effect was tested on the mechanical properties of each CSK component. These tests were performed at two collagenase concentrations (50 and 250 ng/ml) and for a significant level of mechanical stress, i.e., $\sigma_0 = 31$ Pa. As shown in Fig. 7(A), the addition of exogenous collagenases resulted in a significant reduction (by 25%) in elasticity modulus of

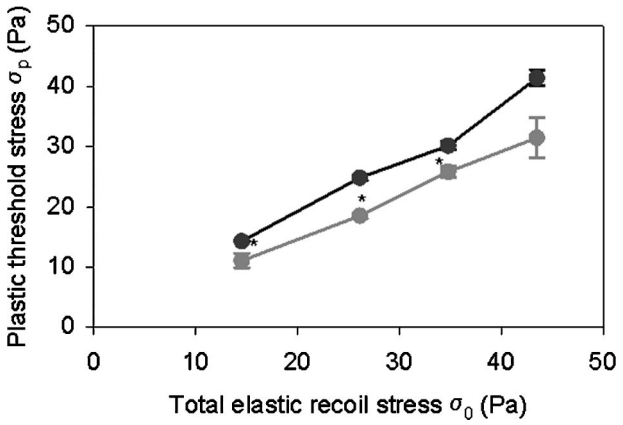

FIGURE 8. Plastic threshold stress σ_p (in Pa) as a function of elastic recoil stress σ (in Pa) without cytochalasin D (dark symbols), with cytochalasin D (gray symbols).

the rapid CSK component. By contrast, no noticeable change in elasticity modulus was observed for the slow CSK component. Moreover, collagenases had no significant effect on the viscosity modulus of the rapid and slow CSK components [see Fig. 7(B)].

Relaxation Period

As soon as the magnetic torque was switched off (period III in Fig. 1), the bead deviation angle θ decreased toward a steady state with horizontal asymptote, which is clearly above the initial bead position (see Figs. 1 and 2). This quite partial recovery of initial bead position (the latter represents the CSK state before loading) reflects a dramatic alteration (or stress induced remodeling) of the CSK structure. In the present model, such a plastic effect has been attributed to the rapid CSK component only because the decay observed during relaxation (period III in Fig. 1) was slow except in the very early phase of relaxation, suggesting that the contribution of the slow CSK component was complete while the contribution of the rapid CSK component was truncated. Note also that, because plastic threshold stress σ_p values remained close to the maximal stress values, most of elastic energy stored in the rapid CSK component was unavailable for relaxation. Another important result is that plastic threshold stress σ_p increased almost linearly with the total elastic recoil stress σ_0 (Fig. 8), which suggests that the higher the stress-induced cellular deformation, the higher the remodeling of the cortical CSK structure. Noteworthy, depolymerization of F-actin by cytochalasin D produced a significant decrease in σ_p at each stress level tested (excepted at $\sigma_0 = 38$ Pa), whereas cytochalasin D treatment did not abolish the positive stress dependency of σ_p.

DISCUSSION

This paper uses magnetic twisting cytometry, i.e., a micromanipulation technique employing coated beads linked to integrin transmembrane mechanoreceptors,[53] to measure the mechanical properties of both the submembranous cortical cytoskeleton and the internal deep CSK in cultured epithelial alveolar cells. To reveal the overall configuration of these two structures within the cell as well as the bead location relatively to each structure, we performed 3D reconstructions of confocal microscopic images of F-actin CSK. The moderately polymerised ''cortical CSK'' surrounds the entire cell while the highly polymerized ''deep CSK'' links large regions of the cytoplasm. Partitioning of mechanical properties of these two types of cytoskeletal components was accomplished by fitting the MTC data with a double viscoelastic solid model with asymmetric plastic relaxation. The results demonstrate that the cortical cytoskeleton responds to the magnetic twisting considerably more rapidly than the deep cytoskeleton. Furthermore, the cortical cytoskeleton is softer, less viscous, and more easily damaged than the deep cytoskeleton. In the conditions used, the actin depolymerizing agent cytochalasin-D primarily affects deep cytoskeletal stiffness without changing cell shape, while collagenase appears to primarily impact cortical stiffness. These observations are largely consistent with the respective functional activity of cortical and deep cytoskeleton, i.e., high sensitivity to the cellular microenvironment for the cortical CSK, and cellular stability for the deep CSK in which actin filaments act interactively with microtubules, intermediate filaments and actin binding proteins.[1,6,17–19,23,30,36]

Experimental evidence that CSK structure is heterogeneous has been observed in living adherent cells including epithelial alveolar cells. These cells are, typically, attached to their substrate through focal adhesion points which converge at a large scale organized network of actin filament assemblies linked to the other networks of biopolymers, e.g., microtubules and intermediate filaments.[17,30] In addition, to ensure anchorage of the cell to the substrate, the CSK structure is given to be determinant for many cellular processes: cell shape, stability, internal tension, and resistance to deformation secondary to external forces.[7,8,26,27] This highly polymerized structure has been thought to be responsible for the ''solid'' viscoelastic response systematically observed in early studies with magnetic twisting cytometry.[43,53,54] As pointed out by Ingber,[24] looking at the CSK structure at a single scale (namely, the cell scale) is far too simplified to account for the multimodular and hierarchical character of the cellular structure. Recently, Fabry *et al.* explored the cellular response over a wide range of frequency and found an infinite number of time constants consistently with the behavior of glassy materials.[14] It

can be said that the present concept emphasizes two of these numerous characteristics time constants, which correspond to two individualized CSK components with quite different structures and functions.

The cortical CSK architecture has already been described in previous studies as a highly branched and prestressed two-dimensional (2D) network, which forms a thin mantle investing the whole cell body[1,6] and maintains an intimate contact of the cell with its mechanical surroundings.[11] Note that smaller values of rigidity and time constant found for the cortical CSK compared to the deep CSK (see Fig. 6 and Table 1) are not inconsistent with enhanced cellular adaptability and fast responsiveness to environmental changes. It is noteworthy that extracellular alterations obtained by degrading extracellular matrix through the action of exogenous matrix metalloproteinases results in a decrease in cortical CSK rigidity. These results explicitly show the role played by molecular interactions with extracellular ligands concerning CSK mechanical properties. Moreover, these results show the sensibility of the cortical CSK to its close environment. In addition, by acting as membrane scaffolding, the cortical CSK allows the cell to assume nonspherical geometries such as those observed in Figs. 3(A) and 3(B). Note that tension in the cortical CSK would be responsible for stiffening of the cell membrane,[12,16] cell functions associated with the plasma membrane such as exocytosis,[32,39] and regulation of stretch-induced calcium signals.[57] This cortical tension could be generated actively through the cell contractile apparatus or passively through osmotic forces acting across cell membrane or, on a smaller scale, by extension forces raised by filament polymerization. We presently found values of CSK prestress (estimated from the decrease in elastic modulus induced by cytochalasin D treatment[41,43]) smaller in the cortical than in the deep CSK. Incidentally, the less dense structure in terms of F-actin concentration, i.e., the cortical CSK component, is less sensitive to F-actin depolymerization than the more dense structure, i.e., the deep CSK component (see the Results).

Values of the cortical CSK time constant (see Table 1) do not fundamentally differ from the recovery time constant of elongated erythrocytes (0.1–0.13 s), early evaluated by Hochmuth *et al.*[21] The time constant value obtained in macrophages using magnetic bead microrheometry,[3] and reanalyzed by Yamada *et al.* (Table 2 in Ref. 58), pertained to the same range (~0.2 s), possibly because the beads, once internalized in the cell, are still connected to a local F-actin CSK.[44] In general, our elasticity modulus values for the cortical CSK are closer, or within, the range of elasticity modulus values obtained for neutrophils tested by cell poker, or leucocytes tested by micropipettes and analyzed either by a homogeneous sphere model[51] or a cortical shell model.[10]

The deep network is a three-dimensional network of interconnected biopolymers, i.e., F-actin, microtubules, intermediate filaments and actin-binding proteins. By contrast to the cortical CSK, the deep actin CSK is organized at the overall cell scale and comprises contractile bundles of actin filaments (stress fibers) which crisscross on the basal surfaces of cells and converge toward focal adhesion plaques located at membrane sites to form either adherent junctions for cell–cell binding or adhesion plaques for adhesion to the underlying substratum. The deep CSK has been shown to serve as a scaffold for organelles and organelle localization[9] and transmits mechanical stresses or biochemical signals toward distal regions, e.g., from the cell membrane to internal organelles such as the nucleus.[27,36] The tensional integrity concept initiated by Ingber[23] predicts that stability of the CSK and its spatial reorganization in response to stress,[50,55] arises because CSK substructures are able to support, even dynamically,[5] opposite efforts such as tension and compression. In terms of overall CSK response, the F-actin network was found to have a major contribution relatively to microtubules, intermediate filaments and linker proteins.[36,52] Present results show that, compared to the cortical CSK, the deep CSK has the longest viscoelastic time constant (see Table 1) that is consistent with the requirement of maintaining the long-term stability of the cell and its adhesion to the extracellular environment. The deep CSK network was found to be stiffer and more viscous than the cortical CSK network (see Fig. 6). This is consistent with a higher level of dynamic filament cross-linking in the cytoplasm and also the cellular distribution of actin bundles, which are thought to reinforce the cell against external mechanical stresses.[46,54] The higher viscosity modulus values of the deep network could be due to the friction of the cross-linked filaments within the cytoplasm, which generally exhibits a very high viscosity modulus.[47] Noteworthy, the deep network exhibits a more marked stress-hardening response than the cortical CSK, likely due to a higher contribution of the spatial rearrangement through a, typically, three-dimensional deep CSK structure.[50,55]

In our tested epithelial cells, the elasticity modulus of deep CSK ranging from 95 to 204 Pa appear closer or similar from those obtained in some other studies. For instance, in cultured endothelial cells evaluated by micropipette aspiration,[47] a mean elastic constant of 140 Pa was found. Interestingly, in these cell cultures, the authors have pointed out the major role of microfilaments in the process of viscoelastic deformation. In epithelial cells evaluated by optical tweezers and using the same bead coating specific to integrins, Laurent *et al.* obtained Young modulus values in the range 29–258 Pa, i.e., right below the deep CSK elastic modulus values reported above.[33] Differences between optical tweezers and MTC concern the type and the amplitude of loading (i.e., a

force parallel to the membrane during laser trapping and a torque during MTC) and the resulting measured deformation (i.e., a translation and a rotation whose respective weight depends on the used micromanipulation technique[33]). The present results suggest that translating the bead would rather result in testing the deep CSK component and to a lesser extent the cortical CSK. The viscosity modulus values for the deep CSK, i.e., (760–2000 Pa×s) appear not really different from values obtained in fibroblasts with magnetic tweezers[3] or microplates. Compared to other studies (see Table 2 in Ref. 58), the values of the elastic and viscosity modulus presently obtained remain generally smaller.

The introduction of plastic relaxation in one of the two components of the viscoelastic model appears to be sufficient to take into account the stress-related damage to the cellular structure likely resulting from bead twisting. It is clear that we consider in our model similar viscoelastic properties, namely, the time constants, between loading and unloading periods for both the cortical and the deep CSK components. If we were assuming that dynamics properties of the cortical CSK are changed from loading to relaxation, e.g., the cortical CSK component response changing from fast to slow, the viscoelastic properties of the deep CSK components would then require to be accordingly modified. We found unrealistic such an assumption because the deep CSK component, which is organized at the overall cell scale and also less easily deformable—the deep CSK is more rigid—appears unlikely modified, as being more protected against damage associated with bead twisting. Then, we assumed unchanged viscoelastic properties between loading and relaxation for both CSK components, the only but important change between these two periods being the addition of the plastic element on the cortical CSK component. Comfirming these assumptions, the results obtained at various stress levels (Table 1) show that the time constants for both deep and cortical CSK components are only slightly altered by the imposed stress while the plastic threshold is markedly increased (almost linearly) as the imposed stress increases (Fig. 8). In summary, the results obtained at different stress levels do not contradict the basic idea of using an asymmetrical model in which the cortical CSK component would carry out the major part of stress-induced alteration and remodeling.

Compared to previous studies, it can be remembered that plastic threshold stress σ_p (Table 1 and Fig. 8) is related to the magnitude of the unrecoverable bead rotation, which is the commonly used parameter in previous MTC studies and which was suspected to depend on F-actin and not microtubules or intermediate filaments.[43,52] The higher σ_p, the larger the unrecoverable bead rotation, and the shorter the time during which the cortical CSK component contributes to relaxation (see Methods). The present results obtained in the relaxation period (70%–80% of the bead deviation angle is not recovered) are similar to those previously obtained by Wang *et al.* in adherent endothelial cells.[52,54] The precise reasons for the inability of the cortical CSK to restitute the stored elastic energy accumulated in the loading phase are not clear. However, the source of permanent deformation likely resembles that for endothelial cells,[52,54] e.g., damage caused to the cellular structure by bead twisting, stress-induced rearrangement, and/or molecular remodeling events. Consistently, alteration of the remodeling process by cytochalasin D presently results in smaller values of σ_p.

Limits of the Model. One may thus wonder whether a single set of five parameters is sufficient and/or pertinent to fit experimental curves during loading and relaxation, i.e., four viscoelastic parameters during loading plus an additional asymmetric plastic parameter during unloading. First, in the present study as classically done in previous studies,[2] we applied the principle of Occams Razor, which states that the simplest model enabling good fitting is considered as the best model for quantitative interpretation of the data. Second, adopting an equivalent mechanical circuit with classical viscoelastic parameters remains the most straightforward way to analyze the viscoelastic response curves. We are aware that the mechanical parameters thereby obtained remain ''apparent'' parameters [Eqs. (7) and (8)]. Indeed, to obtain real (not apparent) values of elastic and viscosity moduli, it is necessary to estimate the spatial stress–strain field in the cellular material from linear theory for continuous mediums, as recently done numerically by Mijailovich *et al.*[38] or any refined structural model associating discrete elements such as tensegrity models.[5,50,55] These three-dimensional approaches are beyond the scope of the present study. Nevertheless, we remember that we have used an analytical correction of the stress based on linear elasticity theory which makes the corrected values of elastic and viscosity moduli closer from real values (see Method and Ref. 33).

The solid-like behavior of the cytoskeletal response might be seen as a controversial result because previous studies of cellular properties with magnetic beads lead to fluid-like behavior.[4] It should be remembered that the fluid-like models tested above failed to provide a satisfactorily curve fitting compared to solid-like models (see Methods). Thus, our results actually differ from those obtained by Bausch *et al.*,[4] most likely because these authors actually measured the mechanical response of cell envelopes comprising the lipid/protein bilayer interfaced with the cytoplasmic fluid in adherent fibroblasts while our beads coated to integrins are precisely related to the CSK structure which would rather resist deformation as a solid, at least in the conditions presently tested.

Let us consider now some reasons explaining why the MTC method is able to evaluate CSK heterogeneity. Based on the spatial reconstructions of the F-actin structure performed in the vicinity of RGD-coated beads [Figs. 4(a)–4(h)], we purposely verified in the present study that, depending on bead location in the cell, a variable fraction of the dense F-actin structure is present in the bead neighborhood. We, however, considered that the properties of the cortical (and deep) CSK components measured at specific locations (the beads) correspond to properties representative of the overall CSK component. On the one hand, each MTC measurement actually reflects a wide spectrum of situations within a cell, (i.e., there are 2 or 3 beads per cell) and between many cells (i.e., about 50×10^3), thus providing an averaged value which means that the MTC method intrinsically smoothes heterogeneities. On the other hand, heterogeneity in the bead deviation angle could modify the response because each bead senses specific cortical and deep CSK properties and rotates with a specific angle.[13,35] To evaluate this effect, we verified that individual bead deviations, estimated over a selected population of beads (e.g., $n=22$), did not totally diverge from the ''overall'' CSK response measured by MTC. Assuming that each bead senses a cortical and a deep elastic modulus in direct proportion with the volume occupied by each type of F-actin substructure (dense and less dense), we have performed a simulation with multiple bead deviations corresponding to a variety of elasticity properties for components Nos. 1 and 2 and the constant viscosity modulus. Surprisingly, the dispersion of curves giving the individual bead rotations remained rather limited; the individual values never differed by more than 25% from those given to analyze the overall MTC response. These results seem to comfirm the ability of the so-modified MTC method to analyze the overall CSK response.

With the magnetic twisting cytometry method, a number of factors contribute to overestimate the bead deviation angle and thus underestimate the viscoelastic properties [see Eq. (7)]: (i) partial bead immersion in the cytoplasm;[33] (ii) heterogeneity in bead deviation angle associated with either heterogeneity in bead immersion (evaluated by Ref. 33) or heterogeneity of the underlying CSK (evaluated in the present study in Figs. 4 and 5); and (iii) heterogeneity in the bead attachment conditions (previously evaluated by Fabry *et al.*[13]). All these factors lead to overestimating the actual bead rotation.

It is noteworthy that the model takes into account one of the specificities of nucleated cells, i.e., the tension generated within the cortical CSK is not directed exclusively toward the membrane equilibrium but is also shared (or resisted) by the three-dimensional deep CSK network that suspends and transmits forces to the elastic nucleus.[18] Similarly, the present results demonstrate that the deep CSK component cannot be considered alone, because the cortical CSK contributes also to the cellular deformation. A recent study demonstrated that fibroblasts show highly localized responses to mechanical deformations.[20] This local accommodation and dissipation of forces was thought to be inconsistent with the proposal that cellular tensegrity determines cell shape according the ''action at a distance'' permitted through the deep CSK, as initially suggested by Ingber.[23,25,37] The proposed two-component model is capable of reunifying apparently opposed experimental observations in which any mechanical deformation is transmitted globally throughout the network, whereas the cell surface is able to ''sense'' very local deformation forces,[20] highly directional forces as well as vibrational sensitivity.[22] The present results reveal that both the cortical and the deep components are tensed [e.g., depolymerization of F-actin significantly decreases the elastic modulus of both CSK components in Figs. 6(A) and 6(B)] and express a stress hardening behavior, suggesting a structural origin for both CSK component behaviors.[55,56] Indeed, theoretical results on the tensegrity model, as well as previous experimental results on epithelial living cells, have shown that the stress hardening response is reduced if the initial tension (prestress) in the structure is decreased, e.g., by cytochalasin D.[43,56]

In addition, we are aware that the type of mechanical coupling between the two CSK components remains questionable. For instance, we cannot ascertain that the cortical and deep CSK components are submitted to the same loading during bead twisting. Moreover, the two components, although very different in shape, cannot be totally independent structures. Indeed, they might have common elements as for as the adherence complex. There might be CSK elements which could be indistinctly in the cortex or the cytosol. Taking the example of stress fibers, they are the actomyosin-based CSK structure observed everywhere in the cytoplasm, which have been shown to link opposite faces of the cell membrane[29] and, thereby, might pertain to both CSK components and/or interconnect the cortical and the deep CSK components. Note that stress fibers were found to behave as truly contractile structures, even once separated from the contractile cell cortex, the cortical CSK, to which they are attached.[28] This suggests that stress fibers predominate in the deep component. Finally, based on recent studies, it appears that the organization of stress fibers is not limited to the basal cytoplasm but can be found in other parts of the cells. Studies on human fibroblasts revealed that, in addition to a number of basal stress fibers interacting with basal membranes, many apical stress fibers interact with the apical plasma membrane.[29]

The proposed two-component viscoelastic model with asymmetric plasticity could appear certainly too simpli-

fied in front of the complexity of CSK structure. Likely, the input signal of the twisting magnetic cytometry method (presently rectangular) explores a limited range of cellular frequencies and cannot really describe the complexity of the CSK response. Note, however, that using two CSK components instead of one does not contradict the recent results by Fabry *et al.*, who found that the cellular response over a wide range of frequency is characterized by an infinite number of time constants in agreement with the behavior of glassy materials near the glass transition.[14]

In summary, in spite of its apparent simplicity in front of the biological complexity, the two-component viscoelastic model with asymmetric plastic relaxation presently proposed constitutes a first step toward a systematic estimation of mechanical CSK heterogeneity. It is based on individual properties of cortical and deep CSK components whose specific biological and functional relevance has been largely documented in the present study.

ACKNOWLEDGMENTS

The authors gratefully acknowledge Antoine Mary and Matthieu Rambaudon for their technical assistance for magnetic twisting cytometry measurements. Two of the authors (R.F. and E.P.) received a grant (ACI Jeunes Chercheurs 2001 No. 2094) from the French Ministry of Research. This study was also supported by the Institut National de la Santé et de la Recherche Médicale (Inserm).

REFERENCES

[1] Albrecht-Buehler, G. Role of cortical tension in fibroblast shape and movement. *Cell Motil. Cytoskeleton* 7:54–67, 1987.

[2] Bausch, A. R., U. Hellerer, M. Essler, M. Aepfelbacher, and E. Sackmann. Rapid stiffening of integrin receptor–actin linkages in endothelial cells stimulated with thrombin: A magnetic bead microrheology study. *Biophys. J.* 80:2649–2657, 2001.

[3] Bausch, A. R., W. Möller, and E. Sackmann. Measurement of local viscoelasticity and forces in living cells by magnetic tweezers. *Biophys. J.* 76:573–579, 1999.

[4] Bausch, A. R., F. Ziemann, A. A. Boulbitch, K. Jacobson, and E. Sackmann. Local measurements of viscoelastic parameters of adherent cell surfaces by magnetic bead microrheometry. *Biophys. J.* 75:2038–2049, 1998.

[5] Cañadas, P., V. M. Laurent, C. Oddou, D. Isabey, and S. Wendling. A cellular tensegrity model to analyze the structural viscoelasticity of the cytoskeleton. *J. Theor. Biol.* 218:155–173, 2002.

[6] Cheng, Y., C. A. Hartemink, J. H. Hartwig, and C. F. Dewey, Jr. Three-dimensional reconstruction of the actin cytoskeleton from stereo images. *J. Biomech.* 33:105–113, 2000.

[7] Chicurel, M. E., C. S. Chen, and D. E. Ingber. Cellular control lies in the balance of forces. *Curr. Opin. Cell Biol.* 10:232–239, 1998.

[8] Choquet, D., D. P. Felsenfeld, and M. P. Sheetz. Extracellular matrix rigidity causes strengthening of integrin-cytoskeleton linkages. *Cell* 88:39–48, 1997.

[9] DePina, A. S., and G. M. Langford. Vesicle transport: the role of actin filaments and myosin motors. *Microsc. Res. Tech.* 47:93–106, 1999.

[10] Dong, C., R. Skalak, K. L. Sung, G. W. Schmid-Schonbein, and S. Chien. Passive deformation analysis of human leukocytes. *J. Biomech. Eng.* 110:27–36, 1988.

[11] Elson, E. L. Cellular mechanics as an indicator of cytoskeletal structure and function. *Annu. Rev. Biophys. Biophys. Chem.* 17:397–430, 1988.

[12] Evans, E., and A. Yeung. Apparent viscosity and cortical tension of blood granulocytes determined by micropipet aspiration. *Biophys. J.* 56:151–160, 1989.

[13] Fabry, B., G. Maksym, R. Hubmayr, J. Butler, and J. Fredberg. Implications of heterogeneous bead behavior on cell mechanical properties measured with magnetic twisting cytometry. *J. Magn. Magn. Mater.* 194:120–125, 1999.

[14] Fabry, B., G. N. Maksym, J. P. Butler, M. Glogauer, D. Navajas, and J. J. Fredberg. Scaling the microrheology of living cells. *Phys. Rev. Lett.* 87:148102, 2001.

[15] Forgacs, G. On the possible role of cytoskeletal filamentous networks in intracellular signaling: An approach based on percolation. *J. Cell. Sci.* 108:2131–2143, 1995.

[16] Glogauer, M., P. Arora, G. Yao, I. Sokholov, J. Ferrier, and C. A. McCulloch. Calcium ions and tyrosine phosphorylation interact coordinately with actin to regulate cytoprotective responses to stretching. *J. Cell. Sci.* 110:11–21, 1997.

[17] Goode, B. L., D. G. Drubin, and G. Barnes. Functional cooperation between the microtubule and actin cytoskeletons. *Curr. Opin. Cell Biol.* 12:63–71, 2000.

[18] Hamill, O. P., and B. Martinac. Molecular basis of mechanotransduction in living cells. *Physiol. Rev.* 81:685–740, 2001.

[19] Hartwig, J. H., and P. Shevlin. The architecture of actin filaments and the ultrastructural location of actin-binding protein in the periphery of lung macrophages. *J. Cell Biol.* 103:1007–1020, 1986.

[20] Heidemann, S. R., S. Kaech, R. E. Buxbaum, and A. Matus. Direct observations of the mechanical behaviors of the cytoskeleton in living fibroblasts. *J. Cell Biol.* 145:109–122, 1999.

[21] Hochmuth, R. M., P. R. Worthy, and E. A. Evans. Red cell extensional recovery and the determination of membrane viscosity. *Biophys. J.* 26:101–114, 1979.

[22] Holley, M. C., and J. F. Ashmore. A cytoskeletal spring in cochlear outer hair cells. *Nature (London)* 335:635–637, 1988.

[23] Ingber, D. E. Cellular tensegrity: defining new rules of biological design that govern the cytoskeleton. *J. Cell. Sci.* 104:613–627, 1993.

[24] Ingber, D. E. Opposing views on tensegrity as a structural framework for understanding cell mechanics. *J. Appl. Physiol.* 89:1663–1670, 2000.

[25] Ingber, D. E., L. Dike, L. Hansen, S. Karp, H. Liley, A. Maniotis, H. McNamee, D. Mooney, G. Plopper, and J. Sims. Cellular tensegrity: Exploring how mechanical changes in the cytoskeleton regulate cell growth, migration, and tissue pattern during morphogenesis. *Int. Rev. Cytol.* 150:173–224, 1994.

[26] Ingber, D. E., D. Prusty, Z. Sun, H. Betensky, and N. Wang. Cell shape, cytoskeletal mechanics, and cell cycle control in angiogenesis. *J. Biomech.* 28:1471–1484, 1995.

[27] Janmey, P. A. The cytoskeleton and cell signaling: Component localization and mechanical coupling. *Physiol. Rev.* 78:763–781, 1998.

[28] Katoh, K., Y. Kano, M. Masuda, H. Onishi, and K. Fujiwara. Isolation and contraction of the stress fiber. *Mol. Biol. Cell* 9:1919–1938, 1998.
[29] Katoh, K., M. Masuda, Y. Kano, Y. Jinguji, and K. Fujiwara. Focal adhesion proteins associated with apical stress fibers of human fibroblasts. *Cell Motil. Cytoskeleton* 31:177–195, 1995.
[30] Kaverina, I., O. Krylyshkina, and J. V. Small. Microtubule targeting of substrate contacts promotes their relaxation and dissociation. *J. Cell Biol.* 146:1033–1044, 1999.
[31] Knauper, V., C. Lopez-Otin, B. Smith, G. Knight, and G. Murphy. Biochemical characterization of human collagenase-3. *J. Biol. Chem.* 271:1544–1550, 1996.
[32] Koffer, A., P. E. Tatham, and B. D. Gomperts. Changes in the state of actin during the exocytotic reaction of permeabilized rat mast cells. *J. Cell Biol.* 111:919–927, 1990.
[33] Laurent, V. M., S. Henon, E. Planus, R. Fodil, M. Balland, D. Isabey, and F. Gallet. Assessment of mechanical properties of adherent living cells by bead micromanipulation: Comparison of magnetic twisting cytometry versus optical tweezers. *J. Biomech. Eng.* 124:408–421, 2002.
[34] Luby-Phelps, K. Physical properties of cytoplasm. *Curr. Opin. Cell Biol.* 6:3–9, 1994.
[35] Maksym, G. N., B. Fabry, J. P. Butler, D. Navajas, D. J. Tschumperlin, J. D. Laporte, and J. J. Fredberg. Mechanical properties of cultured human airway smooth muscle cells from 0.05 to 0.4 Hz. *J. Appl. Physiol.* 89:1619–1632, 2000.
[36] Maniotis, A. J., C. S. Chen, and D. E. Ingber. Demonstration of mechanical connections between integrins, cytoskeletal filaments, and nucleoplasm that stabilize nuclear structure. *Proc. Natl. Acad. Sci. U.S.A.* 94:849–854, 1997.
[37] Mathur, A. B., G. A. Truskey, and W. M. Reichert. Atomic force and total reflection fluorescence microscopy for the study of force transmission in endothelial cells. *Biophys. J.* 78:1725–1735, 2000.
[38] Mijailovich, S. M., M. Kojic, M. Zivkovic, B. Fabry, and J. J. Fredberg. A finite element model of cell deformation during magnetic bead twisting. *J. Appl. Physiol.* 93:1429–1436, 2002.
[39] Muallem, S., K. Kwiatkowska, X. Xu, and H. L. Yin. Actin filament disassembly is a sufficient final trigger for exocytosis in nonexcitable cells. *J. Cell Biol.* 128:589–598, 1995.
[40] Murphy, G., J. A. Allan, F. Willenbrock, M. I. Cockett, J. P. O'Connell, and A. J. Docherty. The role of the C-terminal domain in collagenase and stromelysin specificity. *J. Biol. Chem.* 267:9612–9618, 1992.
[41] Planus, E., S. Galiacy, M. Matthay, V. Laurent, J. Gavrilovic, G. Murphy, C. Clérici, D. Isabey, C. Lafuma, and M. P. d'Ortho. Role of collagenase in mediating *in vitro* alveolar epithelial wound repair. *J. Cell. Sci.* 112(2):243–252, 1999.
[42] Potard, U. S., J. P. Butler, and N. Wang. Cytoskeletal mechanics in confluent epithelial cells probed through integrins and E-cadherins. *Am. J. Physiol.* 272:C1654–C1663, 1997.
[43] Pourati, J., A. Maniotis, D. Spiegel, J. L. Schaffer, J. P. Butler, J. J. Fredberg, D. E. Ingber, D. Stamenovic, and N. Wang. Is cytoskeletal tension a major determinant of cell deformability in adherent endothelial cells? *Am. J. Physiol.* 274:C1283–C1289, 1998.
[44] Qualmann, B., M. M. Kessels, and R. B. Kelly. Molecular links between endocytosis and the actin cytoskeleton. *J. Cell Biol.* 150:F111–F116, 2000.
[45] Raucher, D., T. Stauffer, W. Chen, K. Shen, S. Guo, J. D. York, M. P. Sheetz, and T. Meyer. Phosphatidylinositol 4,5-bisphosphate functions as a second messenger that regulates cytoskeleton-plasma membrane adhesion. *Cell* 100:221–228, 2000.
[46] Satcher, R. L. J., and C. F. J. Dewey. Theoretical estimates of mechanical properties of the endothelial cell cytoskeleton (see comments). *Biophys. J.* 71:109–118, 1996.
[47] Sato, M., D. P. Theret, L. T. Wheeler, N. Ohshima, and R. M. Nerem. Application of the micropipette technique to the measurement of cultured porcine aortic endothelial cell viscoelastic properties. *J. Biomech. Eng.* 112:263–268, 1990.
[48] Small, J. V. The actin cytoskeleton. *Electron Microsc. Rev.* 1:155–174, 1988.
[49] Small, J. V., K. Rottner, I. Kaverina, and K. I. Anderson. Assembling an actin cytoskeleton for cell attachment and movement. *Biochim. Biophys. Acta* 1404:271–281, 1998.
[50] Stamenovic, D., D. E. Ingber, N. Wang, and J. J. Fredberg. A microstructural approach to cytoskeletal mechanics based on tensegrity. *J. Theor. Biol.* 181:125–136, 1996.
[51] Sung, K. L., C. Dong, G. W. Schmid-Schonbein, S. Chien, and R. Skalak. Leukocyte relaxation properties. *Biophys. J.* 54:331–336, 1988.
[52] Wang, N. Mechanical interactions among cytoskeletal filaments. *Hypertension* 32:162–165, 1998.
[53] Wang, N., J. P. Butler, and D. E. Ingber. Mechanotransduction across the cell surface and through the cytoskeleton. *Science* 260:1124–1127, 1993.
[54] Wang, N., and D. E. Ingber. Control of cytoskeletal mechanics by extracellular matrix, cell shape, and mechanical tension. *Biophys. J.* 66:2181–2189, 1994.
[55] Wendling, S., C. Oddou, and D. Isabey. Stiffening response of a cellular tensegrity model. *J. Theor. Biol.* 196:309–325, 1999.
[56] Wendling, S., E. Planus, V. Laurent, L. Barbe, A. Mary, C. Oddou, and D. Isabey. Role of cellular tone and microenvironment on cytoskeleton stiffness predicted by tensegrity model. *Eur. Phys. J.: Appl. Phys.* 9:51–62, 2000.
[57] Wu, Z., K. Wong, M. Glogauer, R. P. Ellen, and C. A. McCulloch. Regulation of stretch-activated intracellular calcium transients by actin filaments. *Biochem. Biophys. Res. Commun.* 261:419–425, 1999.
[58] Yamada, S., D. Wirtz, and S. C. Kuo. Mechanics of living cells measured by laser tracking microrheology. *Biophys. J.* 78:1736–1747, 2000.